Pure Appl. Chem., Vol. 75, No. 8, pp. 1069–1075, 2003.

Molecular porphyrin–fullerene architectures*

Dirk M. Guldi‡

Radiation Laboratory, University of Notre Dame, IN 46556, USA

Abstract: This article describes the utilization of porphyrin and fullerene architectures—yielding artificial light-harvesting antenna and reaction center mimics—to tune the electronic coupling element between electron donor and electron acceptor and ultimately to affect the total reorganization energy. Most importantly, the effects that these parameters have on the rate, yield, and lifetime of the energetic charge-separated states are discussed.

INTRODUCTION

Cascades of short-range energy transfer and electron-transfer events, as they occur between well-arranged light-harvesting antenna ensembles, the photosynthetic reaction center (PRC), and other co-factors, determine the function of natural photosynthesis [1]. The overall small reorganization energy of the PRC, $\lambda \sim 0.2$ eV, and the well-balanced electronic coupling between each component bear key characters for the unique efficiency of natural photosynthesis. Its importance and complexity mandates the design and assembly of artificial systems that efficiently process solar energy, replicating the natural analog [2].

The rich and extensive transitions seen in porphyrinoid systems hold great expectation as light-harvesting building blocks in the construction of molecular architectures, allowing an efficient use of the solar spectrum [3]. Their high electronic excitation energy—typically around 2.0 eV—emerges as a good starting point for a strongly exergonic electron transfer. Note that the latter intercedes the conversion between light and chemical/electrical energy.

C_{60}, which is readily available since the early 1990s, exhibits exciting characteristics as a new 3D electron acceptor. Hereby, the delocalization of charges—both electrons and holes—within the spherical carbon framework together with the rigid, confined structure of the aromatic π-sphere, offers unique opportunities for stabilizing charged entities [4].

Reorganization energy of fullerenes in electron-transfer reactions

The reorganization energy (λ), which is a sum of two terms, inner-sphere reorganization energy (solvent-independent) λ_i, and outer-sphere reorganization energy (solvent-dependent) λ_o, imposes probably the most far-reaching impact on biological electron-transfer systems [5]. In order to achieve small reorganization energies, it is desirable for the construction of photosynthetic models to employ donor–acceptor couples, which offer room for the delocalization of charges.

In C_{60}, contributions from λ_i, which relate to differences in nuclear configurations between an initial and a final state in a chemical reaction, are very small, $\sim 4.3 \times 10^{-5}$ eV [6]. This observation implies that the structure of C_{60} in the ground, reduced, and also excited states is very similar, which relates to the rigidity of these spherical carbon structures. Small Stokes shifts in excitation experiments and small

*Lecture presented at the XIX[th] IUPAC Symposium on Photochemistry, Budapest, Hungary, 14–19 July 2002. Other presentations are published in this issue, pp. 999–1090.

‡E-mail: guldi.1@nd.edu

Raman shifts under reductive conditions lend further support for this conclusion. As far as λ_o contributions are concerned, these are believed to be small as well. The symmetrical shape and large size of the fullerene framework require little energy for the adjustment of an excited or reduced state to the new solvent environment.

The sum of these effects, that is, λ_i and λ_o, bears fundamental consequences upon the classical Marcus treatment of electron-transfer reactions, which predicts that the dependence of electron-transfer rates on the free-energy changes of the reaction, $-\Delta G_{ET}^{\circ}$, yields a parabolic dependence [5]. In the low exergonic region, $-\Delta G_{ET}^{\circ} < \lambda$, an increase in the thermodynamic driving force leads to faster rates ("normal region"), until optimal conditions are reached, when the driving force equals the overall reorganization energy, $-\Delta G_{ET}^{\circ} \sim \lambda$. Then, the highly exergonic region, $-\Delta G_{ET}^{\circ} > \lambda$, is entered, where the rate constants decrease with increasing free-energy changes ("inverted region"). Variation of λ is the key to control the maximum of the parabola. In addition, varying λ influences the shape of the underlying dependence. Hereby, smaller λ values assist in reaching the parabolic maximum at smaller $-\Delta G_{ET}^{\circ}$ values and, in turn, in shifting the energy-wasting charge-recombination deeper into the Marcus "inverted region".

Stabilization of the charge-separated state: Charge-recombination in the inverted region

The choice of planar zincporphyrin (ZnP) and C_{60} as artificial reaction centers helps to reduce the complicated natural mechanism to its basic elements. Excitation of ZnP with visible light leads to its first singlet excited state, ^{1}*ZnP. A rapid *intra*molecular electron transfer (k_{CS}) follows and yields a long-lived charge-separated state—see Scheme 1 [7]. Importantly, a significant fraction (i.e., ~50 %) of the photon energy is converted and stored in form of $ZnP^{\bullet+}$–$C_{60}^{\bullet-}$. A novel fullerene–porphyrin conjugate with van der Waals contacts (*edge-to-edge* separation $R_{ee} \sim 3.0$ Å) provided an exquisite setting for this study. The short separation guaranteed *intra*molecular charge separation in virtually any solvent. In our work, we changed the solvent polarity from toluene to benzonitrile and, thereby, altered the free-energy changes of the electron transfer. Most importantly, a marked acceleration of the charge-recombination rates was seen at smaller $-\Delta G_{CR}^{\circ}$.

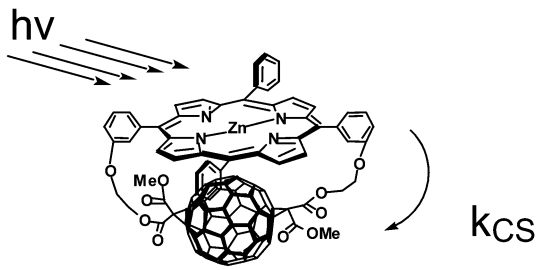

Scheme 1 Schematic illustration of photoinduced charge separation in ZnP–C_{60} dyads.

Comparison of fullerene and naphthalenediimide acceptors

Recently, we reported the first comprehensive assay of λ values for intramolecular electron transfer involving a 3D acceptor (spherical C_{60}) and a 2D acceptor [planar naphthalenediimide (NIm)] [8]. For this purpose, we probed a series of porphyrin-linked C_{60} and NIm ensembles, endowed with similar rigid spacers. Importantly, in all ZnP–C_{60} dyads, the rate of charge separation is much larger than the rate of charge recombination. Conversely, the charge-recombination rate in the corresponding NIm-based dyad, ZnP–NIm, is much larger than the value of charge separation as determined by the picosecond transient absorption spectrum and the decay of the ^{1}*ZnP fluorescence. The λ and V values

are obtained from the intercept and the slope as $\lambda = 0.59 \pm 0.15$ eV and $V = 7.9 \pm 1.7$ cm^{-1}, respectively. A linear correlation was also obtained for ZnP–Nim, which afforded a much larger λ value (1.41 ± 0.33 eV) together with a similar V value (7.8 ± 3.2 cm^{-1}).

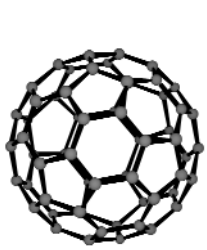

C_{60}

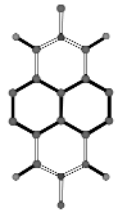

NIm

However, the above conclusion is in sharp contradiction to a hypothesis concerning the λ value for an intermolecular electron self-exchange reaction of *t*-BuC_{60}^{-}/*t*-$BuC_{60}^{\bullet}$. In particular, the value of 0.64 eV in PhCN/benzene (1:7 v/v) is quantitatively similar to that seen for the $BQ^{\bullet-}$/BQ couple (BQ = benzoquinone), 0.74 eV in PhCN. To shed light on this apparent discrepancy, the λ value of intermolecular electron self-exchange between $ZnP^{\bullet+}$/ZnP and between $NIm^{\bullet-}$/NIm were determined by analyzing line width variations in the ESR spectra. The λ values of $ZnP^{\bullet+}$/ZnP and $NIm^{\bullet-}$/Nim were determined from the rate constant in MeCN at 298 K as 0.30 eV and 0.34 eV, respectively. It should be noted that both of these λ values are substantially smaller than the value of *t*-BuC_{60}^{-}/*t*-$BuC_{60}^{\bullet}$ (0.64 eV). With the λ values of the electron self-exchange reaction of each component in hand, the λ values of intermolecular electron transfer were estimated as the average of the two λ values of electron self-exchange reactions. Importantly, the λ value of the intermolecular electron transfer from ZnP to NIm (0.32 eV) is appreciably smaller than what is seen for the ZnP/C_{60} couple (0.47 eV).

Our results clearly infer that intermolecular electron transfer between a NIm acceptor and a ZnP donor takes place at short separation distances rendering the reorganization energy small. In contrast to such a 2D π-system, intermolecular electron transfer involving a spherical 3D π-system (C_{60}) is likely to occur at larger distances. An important asset is the effective radius of the acceptor moiety: Even if C_{60} is held at the same critical distance (i.e., van der Waals contact) as NIm, due to the strong π-π interactions, the effective center-to-center separation is significantly larger. In the case of intramolecular systems, the fixed distance, by which the donor and acceptor are separated, allows to distinguish the intrinsic reorganization energies of a planar and a spherical acceptor. This study has provided valuable insights on the intrinsic reorganization energies of electron transfer, which relate to different molecular shapes.

Donor–acceptor dyads

The first class encompasses linear arrays, in which a systematic variation of the distance R_{ee} separating the donor (ZnP) from the acceptor (C_{60}), to about 11.9 Å leads to lifetimes of up to 2.7 μs in deoxygenated THF [9]. The reorganization energies describe an interesting distance dependence: First, they drop from 0.82 eV at $R_{ee} = 3.0$ Å to ~ 0.5 eV at $R_{ee} = 6.18$ Å, and after that they steadily increase to 0.66 eV at $R_{ee} = 11.9$ Å. The electronic coupling V, on the other hand, decreases monotonically with distance throughout the series from 415 cm^{-1} at $R_{ee} = 3.0$ Å to 3.9 cm^{-1} at $R_{ee} = 11.9$ Å.

Similar effects are also seen for several H_2P–C_{60} dyads. An important consideration implies that the higher oxidation potential of $H_2P^{\bullet+}$/H_2P couple relative to that of $ZnP^{\bullet+}$/ZnP of around 200 mV, would allow storing a larger fraction of the excited-state energy as chemical potential in the charge-separated state.

Donor–acceptor triads and tetrads

Encouraged by these results, several linear triads, R_{ee} = 30.3 Å and tetrads, R_{ee} = 48.9 Å were built around the ZnP/C_{60} couple as artificial reaction centers [9–11]. The first promising results stem from a set of molecular triads in which a fullerene moiety is linked either to an array of two porphyrins (i.e., ZnP and H_2P; ZnP–H_2P) or to a Fc–ZnP fragment [9,10]. In ZnP–H_2P-C_{60}, the ZnP moiety performs as an antenna molecule, transferring its singlet excited-state energy to the lower-lying H_2P. In polar benzonitrile, this energy transfer is followed by a sequential electron transfer yielding ZnP–$H_2P^{\bullet+}$–$C_{60}^{\bullet-}$ and subsequently $ZnP^{\bullet+}$–H_2P–$C_{60}^{\bullet-}$. Considering the overall efficiency of 40 % for (i) funneling light from the antenna chromophore (i.e., ZnP) to the H_2P chromophore, (ii) charge-injection into the fullerene core and (iii) charge-shift, this artificial reaction center reproduces the natural system very well.

The lifetimes of $ZnP^{\bullet+}$–H_2P–$C_{60}^{\bullet-}$ correlate well with the solvent polarity: 34 μs (THF), 21 μs (benzonitrile), 20 μs (DMF) [9]. Since the driving force for charge-recombination, $-\Delta G_{CR}^{\circ}$, decreases even in ZnP–H_2P–C_{60} with increasing solvent polarity the observed trend suggests that the measured rate constants are in the "inverted region" of the Marcus curve.

The function of the Fc–ZnP–C_{60} and Fc–H_2P–C_{60} systems is limited to two consecutive electron transfers yielding the $Fc^{\bullet+}$–ZnP–$C_{60}^{\bullet-}$ and $Fc^{\bullet+}$–H_2P–$C_{60}^{\bullet-}$ in nearly 82 and 25 %, respectively [10]. In oxygen free benzonitrile, $Fc^{\bullet+}$–ZnP–$C_{60}^{\bullet-}$ (1.3×10^5 s^{-1}) and $Fc^{\bullet+}$–H_2P–$C_{60}^{\bullet-}$ (1.2×10^5 s^{-1}) decay, however, considerably faster than what is seen for $ZnP^{\bullet+}$–H_2P–$C_{60}^{\bullet-}$ (4.8×10^4 s^{-1}). Taking into account the similarity in molecular structure and separation, R_{ee} = 30.3 Å, the different thermodynamics must be responsible for this intrinsic behavior. In fact, variation of the $-\Delta G_{CR}^{\circ}$ (i.e., comparing THF and DMF) indicated that the electron-transfer kinetics within the $Fc^{\bullet+}/C_{60}^{\bullet-}$ couples is in the "normal region" of the Marcus relationship.

Successful mimicry of the primary events in photosynthesis using ZnP–H_2P–C_{60} and Fc–ZnP–C_{60} encouraged us to combine these two systems into an integrated single system, Fc–ZnP–H_2P–C_{60}—see Scheme 2 [11]. The lifetime of the spatially separated (R_{ee} = 48.9 Å) radical pair, the product of a sequence of energy and multistep electron-transfer reactions, reaches well beyond milliseconds (0.38 s), into a time domain which has never been accomplished so far in an artificial PRC.

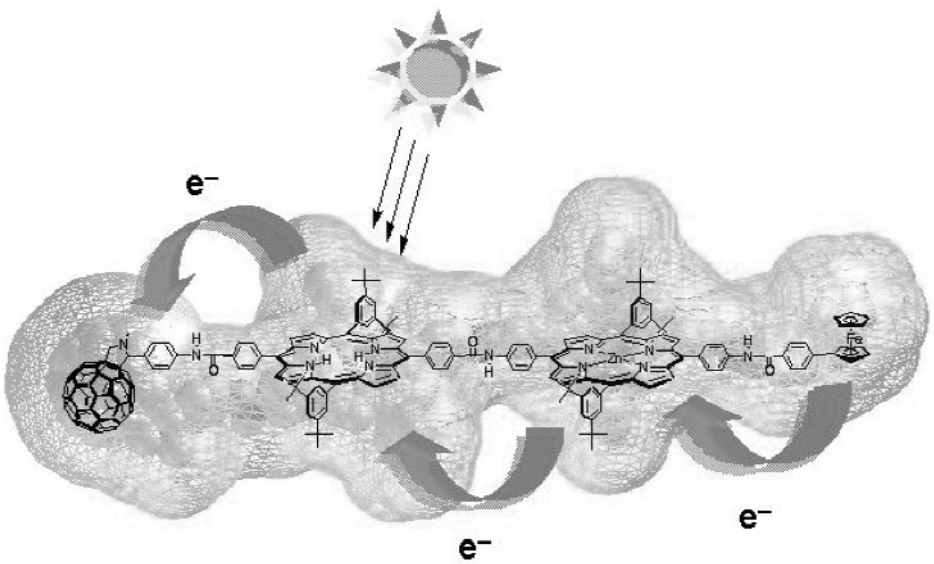

Scheme 2 Sequence of electron-transfer reaction in photoexcited Fc–ZnP–H_2P–C_{60}.

The lifetime is comparable, for example, to the lifetimes of ~1 s in the bacteriochlorophyll dimer radical cation [$(Bchl)_2^{\bullet+}$]-secondary quinone radical anion ($Q_B^{\bullet-}$) ion pair in the bacterial PRC.

Unquestionably, the most striking and far-reaching observation is that charge-recombination in all these $ZnP^{\bullet+}/C_{60}^{\bullet-}$ couples is located in the "inverted region" of the Marcus parabola, regardless of linkage, distance, and orientation. By contrast, lowering the driving force via replacing the ZnP with the better electron donor ferrocene (Fc) shifts the dynamics into the normal region. This variation is of great advantage in determining parameters such as electronic coupling, V, reorganization energy, λ, and damping factor, β, with high accuracy.

Layer-by-layer construction of nanostructured porphyrin–fullerene electrodes

The scope of the following section is our approach to devise electrostatically built nanonetworks that will lead to significant improvements in energy conversion and transport. In particular, the successful construction of photoactive ITO electrodes was accomplished based on a *layer-by-layer* (LBL) approach [12–14]. The strategy, employing porphyrin-linked fullerenes bearing positively charged functionalities, provides several advantages: Firstly, and by far the most important, it allows control over the thickness and composition of the assembled films at the molecular level. Secondly, it guarantees the specific alignment and the orientation of the incorporated donor–acceptor system as a crucial means to facilitate the electron transfer among adjacent layers. Thirdly, repulsion of equally charged substrates restricts each assembly procedure to single-layer coverage.

To visualize the topography of each layer, and to ensure the regularity of the modified electrode surfaces, AFM images were routinely taken after PDDA-, PSS-, and H_2P–C_{60}-coatings to yield the corresponding PDDA/PSS and PDDA/PSS/H_2P–C_{60} films, respectively [14]. In good agreement with our previous results, the structureless assemblies of polyelectrolyte materials are observed for PDDA, PDDA/PSS, etc. Conversely, the subsequent coverage with H_2P–C_{60} gives rise to a completely different image. Not only is the roughness of the surface largely reduced but, relevantly, fine-grained structures of the H_2P–C_{60} layer appear, leading to a continuous uniform film. An important asset is the lack of cluster domains evident on the film surface. On the macroscopic level, close packing within each H_2P–C_{60} layer on top of the PSS template is achieved, as clearly discernable from the AFM images.

Immediately after the preparation, the photoaction spectra of the modified ITO electrodes were recorded under a variety of experimental conditions. An excellent match is noted with the absorption spectrum of the film: the H_2P's *Soret*- and also *Q*-band features are noticeable, while those of C_{60} are masked by the ITO absorption at wavelengths <350 nm.

In conclusion, we have assembled high-quality, robust, and photoactive ITO/H_2P–C_{60} electrodes, making use of electrostatic and van der Waals interactions, which give rise to largely improved light-harvesting features in the visible. In response to visible light irradiation, injection of electrons into the ITO conduction band occurs (i) directly from the photochemically generated $H_2P^{\bullet+}$–$C_{60}^{\bullet-}$ radical pair and (ii) indirectly via electron transport mediated through suitable electron carriers—see Scheme 3. Considering the simplicity and universality of our approach, combined with the useful efficiency found for a monolayer coverage, we believe we have demonstrated a potent alternative in fabricating photoactive molecular devices.

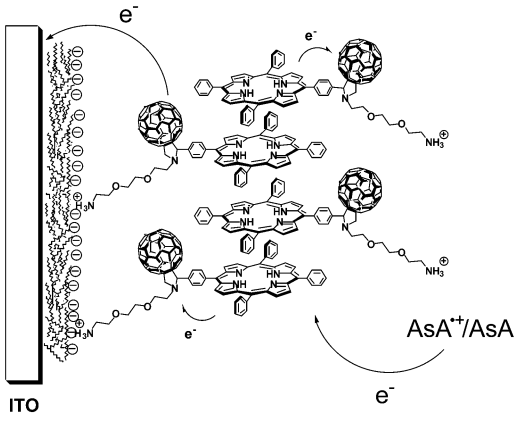

Scheme 3 Schematic illustration of photocurrent generation in ITO electrodes covered with a single-layer film of H_2P–C_{60}.

ACKNOWLEDGMENT

This work was supported by the Office of Basic Energy Sciences of the U.S. Department of Energy. This is document NDRL-4439 from the Notre Dame Radiation Laboratory. I am deeply indebted to Profs. Fukuzumi, Hirsch, Imahori, Maggini, Martin, Prato, and Sakata for their productive collaborations and numerous stimulating discussions.

REFERENCES

1. *The Photosynthetic Reaction Center*, J. Deisenhofer and J. R. Norris (Eds.), Academic Press, New York (1993).
2. *Electron Transfer in Chemistry*, V. Balzani (Ed.), Vols. I–V, Wiley-VCH, Weinheim (2001).
3. *The Porphyrin Handbook*, K. M. Kadish, K. M. Smith, R. Guilard (Eds.), Academic Press, New York (1999).
4. (a) H. Imahori and Y. Sakata. *Adv. Mater*. **9**, 537 (1997); (b) N. Martín, L. Sánchez, B. Illescas, I. Pérez. I. *Chem. Rev*. **98**, 2527 (1998); (c) *Fullerenes and Related Structures*, A. Hirsch (Ed.), Springer, Berlin, Vol. 199 (1999); (d) H. Imahori and Y. Sakata. *Eur. J. Org. Chem*. **64**, 2445 (1999); (e) F. Diederich and M. Gomez-Lopez. *Chem. Soc. Rev*. **28**, 263 (1999); (f) F. Diederich and R. Kessinger. *Acc. Chem. Res*. **32**, 537 (1999); (g) D. M. Guldi. *Chem. Commun*. 321 (2000); (h) D. M. Guldi and M. Prato. *Acc. Chem. Res*. **33**, 695 (2000); (i) D. Gust, T. A. Moore, A. L. Moore. *Acc. Chem. Res*. **34**, 40 (2001); (k) D. M. Guldi. *Chem. Soc. Rev*. **31**, 22 (2002).
5. R. A. Marcus. *Angew. Chem., Int. Ed*. **32**, 1111 (1993).
6. *Fullerenes: From Synthesis to Optoelectronic Applications*. D. M. Guldi and N. Martin (Eds.), Kluwer Academic, Dordrecht (2002).
7. (a) E. Dietel, A. Hirsch, E. Eichborn, A. Rieker, S. Hackbarth, B. Röder. *Chem. Commun*. 1981 (1998); (b) D. M. Guldi, C. Luo, M. Prato, E. Dietel, A. Hirsch. *Chem. Commun.* 373 (2000); (c) D. M. Guldi, C. Luo, M. Prato, A. Troisi, F. Zerbetto, M. Scheloske, E. Dietel, W. Bauer, A. Hirsch. *J. Am. Chem. Soc.* **123**, 9166 (2001).
8. H. Imahori, H. Yamada, D. M. Guldi, Y. Endo, A. Shimomura, S. Kundu, K. Yamada, T. Okada, Y. Sakata, S Fukuzumi. *Angew. Chem., Int. Ed.* **41**, 2344 (2002).
9. C. Luo, D. M. Guldi, H. Imahori, K. Tamaki, Y. Sakata. *J. Am. Chem. Soc.* **122**, 6535 (2000).
10. H. Imahori, K. Tamaki, D. M. Guldi, C. Luo, M. Fujitsuka, O. Ito, Y. Sakata, S. Fukuzumi. *J. Am. Chem. Soc.* **123**, 2607 (2001).

11. H. Imahori, D. M. Guldi, K. Tamaki, Y. Yoshida, C. Luo, Y. Sakata, S. Fukuzumi. *J. Am. Chem. Soc*. **123**, 6617 (2001).
12. C. Luo, D. M. Guldi, M. Maggini, E. Menna, S. Mondini, N. A. Kotov, M. Prato. *Angew. Chem., Int. Ed.* **39**, 3905 (2000).
13. D. M. Guldi, C. Luo, D. Koktysh, N. A. Kotov, T. Da Ros, S. Bosi, M. Prato. *Nano. Lett.* **2**, 775 (2002).
14. D. M. Guldi, F. Pellarini, M. Prato, C. Granito, L. Troisi. *Nano. Lett.* **2**, 965 (2002).